Journal of Neuroscience Methods 199 (2011) 108–118

Contents lists available at ScienceDirect

Journal of Neuroscience Methods

journal homepage: www.elsevier.com/locate/jneumeth

Detecting overlapped functional clusters in resting state fMRI with Connected Iterative Scan: A graph theory based clustering algorithm

Xiaodan Yan[a,b,*], Stephen Kelley[c], Mark Goldberg[c], Bharat B. Biswal[d]

[a] Cognitive Science Department, Rensselaer Polytechnic Institute, Troy, NY 12180, USA
[b] Center for Neural Science, New York University, New York, NY, 10003, USA
[c] Computer Science Department, Rensselaer Polytechnic Institute, Troy, NY 12180, USA
[d] Department of Radiology, UMDNJ-New Jersey Medical School, Newark, NJ 07103, USA

ARTICLE INFO

Article history:
Received 19 November 2010
Received in revised form
30 November 2010
Accepted 1 December 2010

Keywords:
Clustering
Resting state fMRI
Graph theory
Brain network
Hub

ABSTRACT

The brain is a complex neural network with interleaving functional connectivity among anatomical regions. However, current functional parcellation algorithms usually emphasize independence or orthogonality between the spatial components, with the interleaving nature underrepresented. This study investigates a method, Connected Iterative Scan (CIS), for identifying functionally overlapped anatomical groups with resting state fMRI. CIS iteratively optimizes a grouping of vertexes in a weighted graph, using a density metric computed based on the input and output weights of a candidate cluster. In this study, CIS is able to detect the overlapped clusters in a simulated dataset. CIS also detects that the default mode network and the task positive network, which were known as two anti-correlated networks, are overlapped at the posterior cingulate cortex and the lateral parietal cortex. CIS also detects the conventional functional clusters in the whole brain neural network (e.g., the visual cluster, the motor cluster, the frontal cluster, etc.), as well as meaningful overlaps, and also revealed the possible existence of an emotional memory functional cluster. CIS was able to identify several hub regions actively participating in many clusters. With the ability to reveal overlapping functional clusters, CIS is potentially useful in revealing the delicate architecture of the brain neural network.

1. Introduction

In resting state fMRI, while subjects are not performing any prescribed cognitive tasks, functionally related brain regions have been observed with significant temporal correlations originating from the synchronization of low frequency spontaneous oscillation (Biswal et al., 1995, 1997, 2010). The concept of functional connectivity has been applied to resting state fMRI to capture this temporal synchronization (Friston, 1994) in the resting state network (RSN). Many methods have been developed to analyze the functional connectivity, such as hypothesis-based analysis or data-driven methods. Smith and colleagues have published a comprehensive summation on these methods (Cole et al., 2010).

A common approach for these analyses has been to select an appropriate seed voxel or seed region based on a research interest, correlate the average signal from the seed with all other voxels in the brain, and determine the statistical significance of the correlation (Biswal et al., 1995; Cordes et al., 2000a; Li et al., 2000; Stein et al., 2000; Margulies et al., 2007). This approach, although simple to implement and popular in usage, is subject to researcher bias in the selection of region of interest (ROI) (Friston et al., 2006).

Data-driven methods have also been developed as an effort to capture the intrinsic connectivity in RSN without researcher bias. These methods include clustering methods (Goutte et al., 1999; Cordes et al., 2000a, 2002; Stanberry et al., 2003; Golland et al., 2008; Morgan et al., 2008), principle component analysis (PCA) and independent component analysis (ICA) (McKeown et al., 1998; Oja and Hyvarinen, 2000; Calhoun et al., 2003; Smith et al., 2009). Recently there are some attempts to detect the communities among the neural network in the brain (Fortunato, 2009; Lancichinetti and Fortunato, 2009; Lancichinetti et al., 2010). All of these methods are based on the assumption that the neural network in the brain consists of several orthogonal or statistically independent components and aim to dissociate these components. Specifically, the assumption is made that functional components are disjoint from one another. However, this assumption may not be strictly justified. Unlike anatomical brain regions, the boundaries between the functional clusters in the brain network may not be clearly demarcated. Many brain regions have been found with multiple functions and should be considered to participate in many functional clusters. Therefore, it is meaningful and worthwhile to investigate functional

* Corresponding author at: Cognitive Science Department, Rensselaer Polytechnic Institute, Troy, NY 12180, USA. Tel.: +1 518 892 0064.
E-mail address: xiaodan.yan@yahoo.com (X. Yan).

0165-0270/$ – see front matter © 2011 Elsevier B.V. All rights reserved.
doi:10.1016/j.jneumeth.2011.05.001

clusters with the ability to detect any spatial overlap among them.

This study makes use of a graph-theoretic clustering algorithm, called Connected Iterative Scan (CIS). The algorithm was previously developed and applied successfully in inter-personal social networks to detect and analyze overlapping communities. In social networks, such communities are common, since many people are involved in more than one groups reflecting their various interests (Baumes et al., 2008; Goldberg et al., 2008, 2010). CIS starts by taking each vertex of the graph as a candidate set and attempting to add/delete each other vertex into the set as suggested by a density metric based on the input and output weights of the whole set. Changes in the cluster's membership are made only if the addition or removal of the vertex results in an increase of the density metric. This process continues iteratively until neither the addition nor removal of a vertex results in an increase in the density metric. Connectivity is maintained by checking for disconnection following each iteration. When connectivity is not maintained, the optimization proceeds on only the highest density connected component of the original set. This routine is run on each of the candidate sets, and upon completion, all unique, locally optimal sets are considered to be final clusters. In the fMRI data, preprocessed fMRI time series give rise to cross-correlation matrices. Correlation coefficients above a certain threshold are taken as weights on the edges of the graphs (Fig. 1).

In order to test the efficacy and sensitivity of CIS, simulated data was generated. The performance of CIS is also compared with the *K*-means clustering method, a traditional clustering method that does not allow for overlap between the resulting clusters and requires that the desired number of clusters be specified. Two specific brain networks are investigated using CIS and compared with the *K*-means clustering method. The first brain network (Set 1) containing 31 vertices representing two well-known anti-correlated sub-networks in RSN as reported in previous studies (Fox et al., 2005; Toro et al., 2008); The second brain network (Set 2) consists of 90 vertexes representing anatomical regions across the whole cerebral cortex. The ground truth for this network relies on a previously published template (Tzourio-Mazoyer et al., 2002) widely used in graph theoretical based analysis in fMRI (Achard et al., 2006; Achard and Bullmore, 2007; Supekar et al., 2008, 2009; Gong et al., 2009; Wang et al., 2009). The goal of this study is to investigate if CIS can replicate the known dissociation and also reveal possible overlap between the two anti-correlated networks in Set 1. We also investigate its ability to detect the well-known functional clusters in Set 2 and to reveal possible overlap among them. In all the datasets, we compare the results of CIS and *K*-means.

2. Method

2.1. Simulation dataset

2.1.1. Dataset generation

In order to test the validity of the proposed clustering method, analysis of a simulated dataset was performed. A data matrix was generated using a linear combination of 2 random vectors x, y with 2000 time points in each. A temporal delay of up to 10 time points was used in this study to account for the hemodynamic delays typically observed in fMRI studies (Saad et al., 2001; Biswal et al., 2003). Noise was also introduced to vary the weighting between the two vectors in the linear combination. Thus we obtained 9 vectors with 6 describing the original signal and the delay of each signal and another 3 describing the linear combination:

$$\begin{aligned} &x = rand_1; y = rand_2;\\ &delay = ceil(abs(rand_3) * 5)\\ &X = [x, x + delay, x - delay];\\ &XY = [w_1x + w_2y, w_1x + w_2y + delay, w_1x + w_2y - delay];\\ &Y = [y, y + delay, y - delay];\\ &w_1 = rand_4 * 0.001 + 0.5; w_2 = rand_5 * 0.001 + 0.5. \end{aligned} \tag{1}$$

And the final dataset was constructed as

$$M = [X, XY, Y]; \tag{2}$$

Therefore, $M_{2000\times 9}$ has three components which were generated to have overlap between them.

In order to test the robustness of the clustering algorithms, we generated 10 such datasets by regenerating the random numbers in (1). Noise was added to M by adding a random number to each element of M to generate M_2 (Fig. 2A). The following clustering algorithms were performed on each implementation of M and M_2.

2.1.2. Clustering with CIS

A weighted graph was constructed by considering each column of M as a vertex and the correlation coefficients between each pair of the 9 vertices as the weights on the edges between them

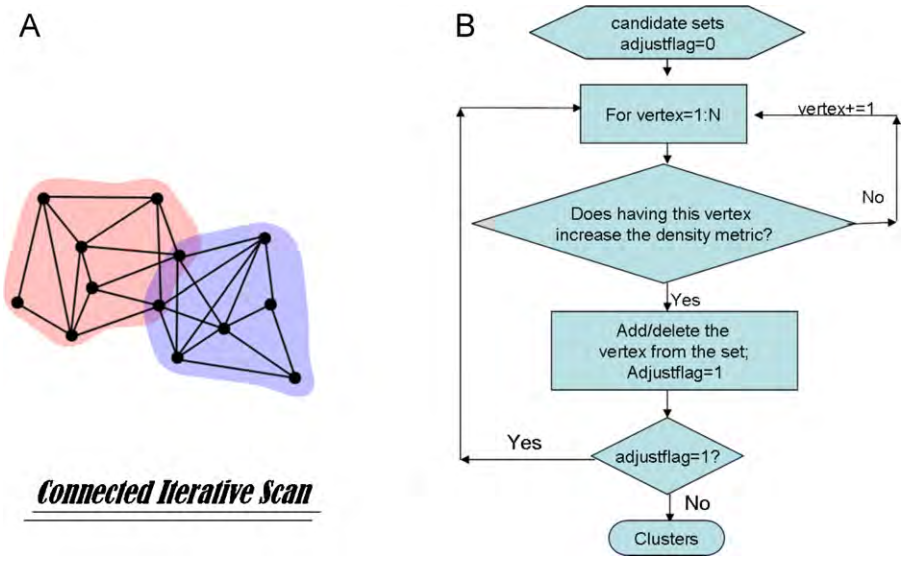

Fig. 1. The illustration of Connected Iterative Scan. (A) Illustration of the overlapping clusters. (B) Illustration of the procedure of the algorithm.

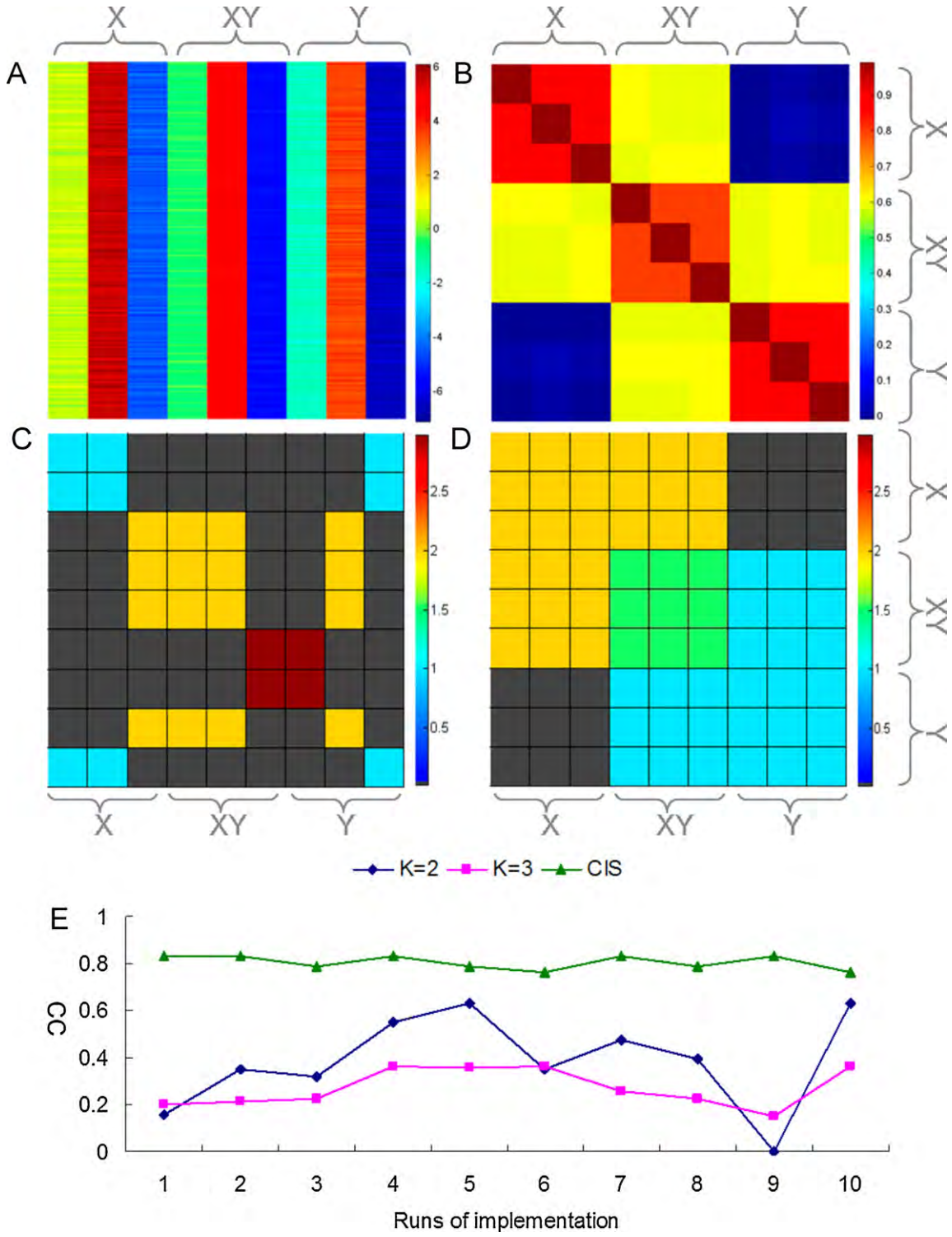

Fig. 2. The clustering results on the simulation dataset. (A) The original data. (B) Correlation coefficients among the 9 vectors. (C) Clustering results from *K*-means. (D) Clustering results from CIS. (E) The robustness of performance of *K*-means ($K = 2$ and $K = 3$) and CIS over 10 implementation of the simulation dataset (M) with random noise. The robustness was measured by the correlation (CC) of output cluster results from M and M with additional random noise on each of its elements (M_2).

(Fig. 2B). CIS starts by taking each vertex as a candidate set, and it iterates though each of all other vertices, attempting to add or remove the vertex from the set if such changes could increase the density metric. This continues until no vertices, when added or removed, result in an increase in density metric of the candidate set. This routine is run on each of the candidate sets, and upon completion, all unique, locally optimal sets are considered as clusters.

Selecting an appropriate density metric is important to CIS. Traditionally, the density metric defined as

$$\text{Density} = \frac{w_{in}}{w_{in} + w_{out}} \tag{3}$$

has been used for social networks, where w_{in} is the sum of weights (which is the standardized correlation coefficient) of all edges internal to the cluster and w_{out} is the sum of weights of all edges

which connect vertexes in the cluster to vertexes outside the cluster. However, in the brain network, whose connections are much denser than social networks, this is inappropriate since clusters are encouraged to grow to include the whole graph. Therefore, we consider a new density function paired with a filtering of edge weights give as

$$\text{Density} = \frac{w_{in}}{w_{in} + w_{out}} + \lambda * \frac{2 * w_{in}}{c * (c-1)} \quad (4)$$

where c is the size of the cluster being examined. The second term in the function penalizes those groups which do not have high values of pair wise correlation within the vertex set, to prevent clusters from growing too big. Edge probability (EP) is defined as

$$\text{EP} = \frac{2 * w_{in}}{c * (c-1)}. \quad (5)$$

The first term in the density metric reflects how isolated a cluster is from other elements in the whole data set, while the EP metric reflects the level of connectedness of the cluster.

2.1.3. Clustering with K-means

To serve as a reference, we also applied the *K*-means clustering method. The correlation coefficients between the 9 vectors were used as measurements of distances. The *K*-means clustering algorithm has two phases: in the first phase, each point is assigned to its nearest cluster centroid in the dataset, followed by recalculation of the cluster centroids; in the second phase, the points are reassigned if doing so can reduce the sum of distances, and cluster centroids are recalculated after each reassignment. Such a process iterates through all points in the dataset (Spath, 1985). We used the implementation in the Matlab statistics toolbox for this analysis (The MathWorks, Natick, MA), setting *K* to 2 and 3.

2.2. Biological dataset

2.2.1. Data acquisition

A 7 min resting state fMRI scan and an accompanying high resolution anatomical scan was obtained from 30 normal subjects. The subjects were instructed not to move during the scanning session. They were instructed to relax, breathe normally, and refrain from systematic thinking on anything in particular. The subjects did not have any history of neurological or psychiatric disorders. The experimental protocol was approved by the Research Ethics Review Board of the Institute of Psychology, Chinese Academy of Sciences. Written informed consent was obtained from each participant.

Structural and functional images were acquired on a GE 3.0 T Signa Excite Gemse MRI system (GE Healthcare, Milwaukee, WI, USA) at Huaxi Magnetic Resonance Research Center (West China Hospital, Chengdu, China). 3D structural MRI was acquired from each subject using a T1-weighted MPRAGE sequence (TR/TE = 8.5 ms/3.4 ms, TI = 400 ms, FOV = 28 cm, flip angle = 12°), yielding 156 contiguous axial slices (1 mm thick) covering the whole brain. Resting state BOLD fMRI was obtained with an EPI sequence (TR/TE = 2000/30 ms, FOV = 24 cm × 24 cm, flip angle = 90°). 200 volumes of 28 contiguous axial slices at 5 mm thickness (without gaps) covering the whole brain were acquired from each subject (subjects were instructed to remain awake with their eyes closed). The original voxel size was 3.75 mm × 3.75 mm × 5 mm.

2.2.2. Data preprocessing

The individual anatomical data was normalized to Talairach and Tournoux space (Talairach and Tournoux, 1988). The following pre-processing was performed on each individual's functional data: discarding the first 10 volumes for scanner calibration, slice timing, motion correction, removal of linear drift, smoothing with a Gaussian filter of 6 mm FWHM, and registration to its corresponding normalized anatomical data. A regression analysis was conducted with the following regressors: the estimated profiles of head motion (three for translation and three for rotation), the average time series from white matter and CSF, therefore to remove identifiable variance in the BOLD signal (Fox et al., 2005). The residuals from the regression were then used for the following analysis. None of the subjects' head motion in any direction exceeded one voxel, so no subject was excluded.

2.2.3. Graph generation

2.2.3.1. Set 1. Previously a meta-analysis published 31 peak locations of two anti-correlation networks in resting state (Toro et al., 2008); we extracted the mean time series from four voxels surrounding the reported coordinates in that study and constructed a symmetric correlation matrix of Pearson's correlation coefficients (r) for each subject. The 31 by 31 matrix of each individual was transformed via Fisher r–z transformation (Fisher, 1915) to allow for averages to be taken across the whole group. After the Fisher r–z transformation, we calculated the group average Z-transformed correlation coefficients (R-matrix) as well as the corresponding standard deviation (SD-matrix). By having each element in the R-matrix divided by the corresponding element in the SD-matrix, we further obtained the normalized group average Z-matrixes which are shown in Fig. 4C. We further threshold the Z-matrix to construct the adjacency matrixes in the following ways for three kinds of graphs:

(1) $r \leq T$ ($T = -0.5$ to -0.1), with corresponding graphs called *Negative Network*.
(2) $r \geq T$ ($T = 0.1$–0.5), with corresponding graphs called *Positive Network*.
(3) $|r| \geq T$ ($T = 0.1$–0.5), with corresponding graphs called *Absolute Network*.

Note: The r scores were transformed to z scores also with the Fisher r–z transform, and the threshold (T) values were used at a 0.1 step, i.e., 0.1–0.5 means 0.1, 0.2, 0.3, 0.4, 0.5.

The adjacency matrices were further weighted with the standardized correlation coefficient (Z scores), to created a weighted graph for CIS. The reasons for thresholding the graphs are discussed in Section 3.

2.2.3.2. Set 2. The functional data was parcellated into 90 anatomical regions using the anatomical automatic labeling (AAL) template (Tzourio-Mazoyer et al., 2002). Mean time series were extracted from each of the regions, and a symmetric correlation matrix for each subject was constructed with the Pearson's correlation coefficients (r) between each pair of regions. The 90 by 90 matrix of each individual was transformed via Fisher r–z transformation (Fisher, 1915) to allow for averaging across the whole group. We also obtained the R-matrix, the SD-matrix and the Z-matrix, as well as the three kinds of graphs (*Negative Network*, *Positive Network* and *Absolute Network*) with the same methods as we used on Set 1. For the purpose of visualization, we averaged the time series of the left and right sides of each anatomical region, and obtained the corresponding 45 by 45 matrixes with the same methods. These are shown in Fig. 5C. The adjacency matrix was also weighted with the standardized correlation coefficient (Z scores), to create a weighted graph for CIS.

2.2.4. Clustering with CIS

The same processing as in the simulation dataset (Section 2.1.3) was applied on the two biological datasets. Furthermore, based on the degree of overlap between the clusters, we detected justified pairs (JPs) of overlap with the overlap elements constituting

10–90% of either cluster. Pairs with the overlap taking up above 90% of either cluster were merged into one cluster.

We further identified hub regions with the hub index defined as

$$Index_{Hub} = \left(\sum_{|T|}^{K} freq(JP_T) * \left|\frac{T}{10}\right|\right) * \left(\bigcap_{|T|}^{K} freq(JP_T)\right) \quad (6)$$

where T is the threshold on the Z-matrix for generating graphs. $K = 5$ for the graph from the positive network and $K = 3$ for the graph from the negative network. A region was considered as a hub region only if it occurred in a JP among the clustering results of graphs from all thresholds under investigation; because if for any T, $freq(JP_T) = 0$ will result in a 0 value for the second factor of (6), further resulting in a 0 value for the $Index_{Hub}$. The contribution of JP from graphs at different thresholds was weighted accordingly. Compared to previous direct graph theoretical measurements in determining the hub regions, the above criteria is very stringent.

2.2.5. K-means clustering

The same algorithm as in the simulation dataset (Section 2.1.3) was applied here. Numbers of clusters ("K") for each dataset were set based on the cluster numbers from CIS, i.e., $K_{set1} = 3$ and $K_{set2} = 6$.

3. Results

3.1. Simulation set

3.1.1. Cluster results presentation algorithm

In order to present the clustering results vividly, we constructed a symmetric matrix $N_{9\times9}$ with cluster identifications (ID). The clusters were ranked with their sizes, and the smallest cluster was given ID_1 and the largest cluster was given ID_d. For each pair of elements $(c_{i,k}, c_{j,k})$ in a cluster ID_k, N_{c_i,c_j} was assigned the value ID_k. For elements participating in more than one clusters, the value was the addition of half of the new cluster ID and the existing values at that element, i.e.,

$$N_{c_i,c_j} = \begin{cases} ID_k (N_{ci,cj} = 0) \\ (M_{ci,cj} + ID_k) * 0.5 (N_{ci,cj} \neq 0) \end{cases} (k = 1, 2, \ldots, d) \quad (7)$$

3.1.2. Clustering results

The clustering algorithms were performed on each realization of M and M_2, with M_2 being the matrix with noise added to M. In order to test the robustness of the clustering algorithms, we correlated the corresponding matrix with the cluster results N and N_2, and obtained CC as defined in (8), i.e., the average of the absolute values of the correlation coefficients of the whole matrix, with a higher value indicating greater robustness of the algorithm.

$$CC_m = mean(abs(corr(N, N_2))), m = 1, 2, \ldots, 10 \quad (8)$$

In most cases, CIS output two clusters [X, XY], [XY, Y], reflecting the intrinsic overlap in the dataset (Fig. 2D). Additionally, the output of CIS is very robust and consistent (Fig. 2E). The output of K means is relatively not robust and not consistent (Fig. 2E), with a typical output being presented in Fig. 2C, which breaks apart the intrinsic components in the data.

3.2. Biological dataset

3.2.1. Threshold effect

The reason for thresholding the Z matrix is to explore the proper criteria for determining the existence of an edge in the graph. The effect of different thresholds on the clustering results is demonstrated in Fig. 3. As the figure shows, the threshold of 0.3 on the positive network gave reasonable cluster size and cluster number. The clustering results using this threshold are plotted below (Figs. 4 and 5). All thresholds were considered when identifying hub regions.

Table 1
The clustering results and ROI membership in dataset 1. $K = 2$: output from the K-means clustering method with cluster number specified as 2. CIS: output from the Connected Iterative Scan method.

ROI	Ref*	$K = 2$	CIS
IPS-L	p	C1	C3
IPS-R	p	C1	C3
vIPS-L	p	C1	C3
vIPS-R	p	C1	C3
FEF-L	p	C1	C3
FEF-R	p	C1	C3
iPCS-L	p	C1	C3
SMA/preSMA	p	C1	C3
DLPFC-R	p	C2	C2,C3
vOC-L	p	C1	C3
vOC-R	p	C1	C3
aIns-L	p	C1	C3
aIns-R	p	C1	C3
aIns-R2	p	C1	C3
vFEF-L	p	C2	C1,C2
vFEF-R	p	C1	C3
vOC-L2	p	C2	
Th-L	p	C2	C1,C3
Cb-R	p	C2	C1,C2
pCC1	d	C2	C1,C2,C3
pCC2	d	C1	C1,C2,C3
LPC-L	d	C2	C1,C2,C3
aCC1	d	C2	C1,C2,
aCC2	d	C2	C2
SFC-L	d	C2	C2
SFC-R	d	C2	C2
iTC-R	d	C2	C2
paraHipp-L	d	C2	C1
paraHipp-R	d	C2	C1
NA	d	C2	C1,C2
iTC-R2	d	C2	C1,C2

3.2.2. Cluster results of Set 1 with CIS

In this dataset, CIS was able to detect the two clusters that were previously differentiated as a *task-positive network* (cluster 3 in Table 1) and a *default mode network* (cluster 2 in Table 1); we also found that vFEF-L, Cb-R of the *task-positive network* and pCC1,pCC2,LPC-L, DLPFC-R of the *default mode network* are the overlapping elements of the two clusters. Additionally, CIS also identified a sub-cluster of the *default mode network*, which is overlapped with the *task-positive network*.

3.2.3. Cluster results of Set 2 with CIS

6 clusters were identified in this dataset. They were highly overlapped with each other, including a hippocampus & amygdala cluster (cluster 1 in Table 2), a visual cluster (cluster 2 in Table 2), a motor–somatosensory cluster (cluster 3 in Table 2), as well as a frontal–cingulate cluster (cluster 4 in Table 2). It was discovered that cluster 1 and cluster 2 were overlapped at the fusiform cortex, cluster 2 and cluster 3 were overlapped at the superior parietal cortex, and cluster 2 and cluster 4 were overlapped at the precuneus. This might indicate that the fusiform cortex is critical for the communication between the hippocampus & amygdale system and the visual network, the superior parietal cortex is critical for the communication between the visual network and motor–somatosensory network, while the precuneus is critical for the communication between the visual network and the frontal–cingulate network.

A frontal–temporal cluster was identified (cluster 6) which overlaps with the frontal–cingulate cluster (cluster 4). The primary sensory regions (precentral cortex, postcentral cortex, olfactory cortex, fusiform cortex and angular cortex) were grouped together as the hippocampus and parahippocampal cortex, the amygdala,

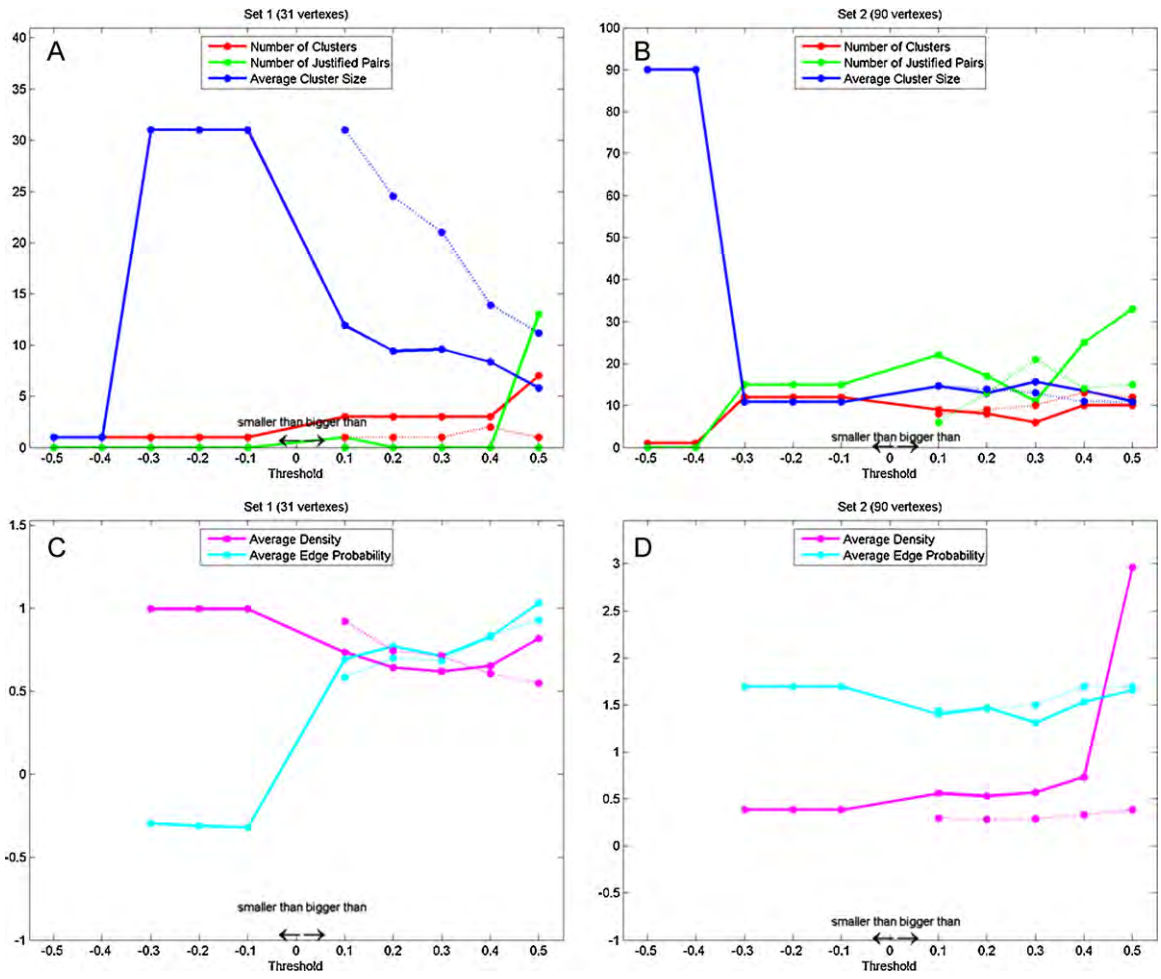

Fig. 3. Clustering output parameters across different thresholds. The thresholds were used as defined for the three networks in Section 2. The dashed lines stand for measurements of corresponding colors shown in the legend, but from the absolute network. Thresholds were chosen based on the appropriateness of the clustering results, thresholds with ill outputs (e.g., outputting only 1 cluster) were not used in further analysis. (For interpretation of the references to color in this figure legend, the reader is referred to the web version of the article.)

the insula and the middle and inferior frontal cortex (cluster 5), which might indicate the existence of a network consisting of the primary sensory regions and the hippocampus–amygdala system as well as the frontal cortex, serving for certain important functions such as the formation and consolidation of emotional memory.

3.2.4. *Hub regions in the whole brain network (Set 2)*

In the whole brain network (Set 2), the parcellated regions in the frontal cortex, the parietal cortex and the visual system served as hub regions, as well as the both the anterior cingulate cortex and the cuneus (Fig. 6; Table 3). We identified such regions in the brain

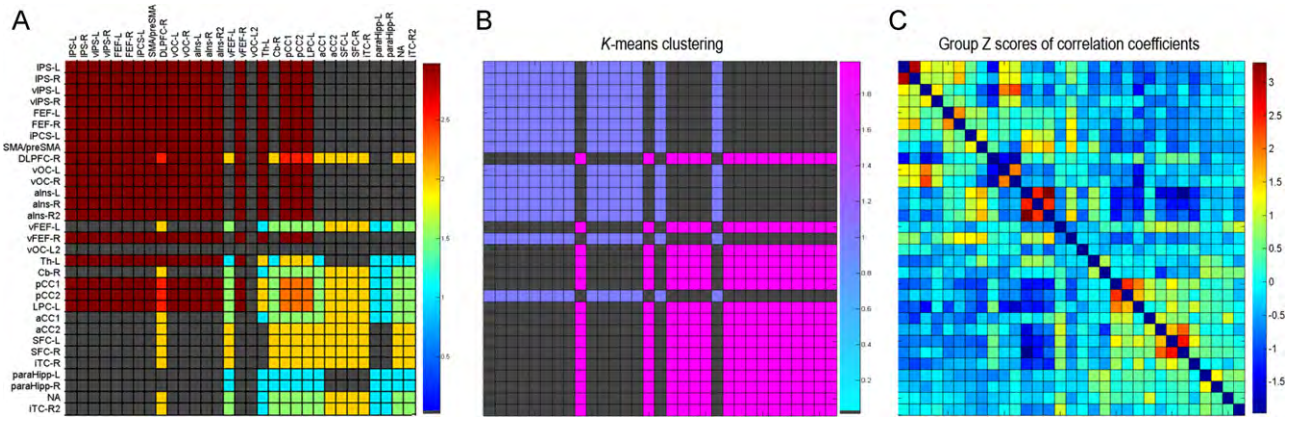

Fig. 4. (A) Cluster results of Set 1 (31 vertexes). Colors labeled the cluster IDs in Table 1. If an element is the overlap between two or more clusters, it will be set to an intermediate color. Refer to Table 1 for detailed clustering results and explanation of the abbreviations. (B) Cluster results of *K*-means clustering algorithm. Colors are labeled in the same way as in (A). (C) The matrix of group average correlation coefficients, in the form of *Z* scores, which is the matrix based on which graphs were generated for CIS. We can see blurry clusters in such raw data. (For interpretation of the references to color in this figure legend, the reader is referred to the web version of the article.)

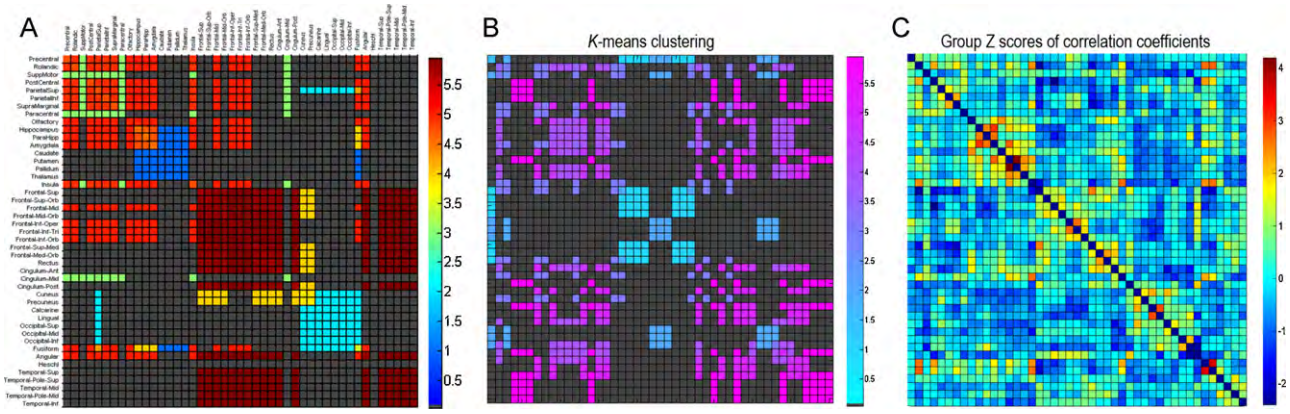

Fig. 5. (A) Cluster results of the whole brain dataset. Colors labeled the cluster IDs in Table 2. If an element is the overlap between two or more clusters, it will be set to an intermediate color. Refer to Table 2 for detailed clustering results. (B) Cluster results of *K*-means clustering algorithm. Colors are labeled in the same way as in (A). (C) The matrix of group average correlation coefficients, in the form of *Z* scores, which is the matrix based on which graphs were generated for CIS. We can see blurry clusters in such raw data. *Note*: To facilitate illustration, the left and right sides of corresponding anatomical region were merged into one element in each of the three figures. (For interpretation of the references to color in this figure legend, the reader is referred to the web version of the article.)

atlas to demonstrate their locations (Fig. 7). No hub regions were identified in Set 1 because there were no JPs across all thresholds (see Fig. 3A).

For comparison, we also plotted the degrees of each region (i.e., the number of edges from a vertex in a graph) as shown in Fig. 8. We can see that the motor and somatosensory areas, the olfactory cortex have degrees above one standard deviation from the algorithm average (however, since the degree distribution is not normal (the right curve on the right side of Fig. 8), the use of algorithm average and standard deviation is only putative rather than strictly reflecting the sample), together with the amygdala and the caudate. Previous studies have reported strictly defined hub regions in terms of the shorted regional path length, and most of the hub regions identified in the current study were previously reported (Table 3).

4. Discussion

In the current study, a graph-theoretic based clustering algorithm, *Connected Iterative Scan* (CIS), was applied to analyze the functional connectivity in the brain network formulated via resting state fMRI data. Unlike traditional clustering methods, CIS allows for identified clusters to overlap. Results from the simulation dataset confirmed that CIS outperforms *K*-means in terms of the robustness and consistency, as well as the capability to capture the overlap between functional clusters. In RSN, CIS successfully detected the two anti-correlated networks, as well as functional clusters including the visual cluster, the motor–somatosensory cluster, the amygdala–hippocampus cluster, and the frontal–cingulate cluster. CIS also detected overlaps between them, a dimension previously ignored by other methods.

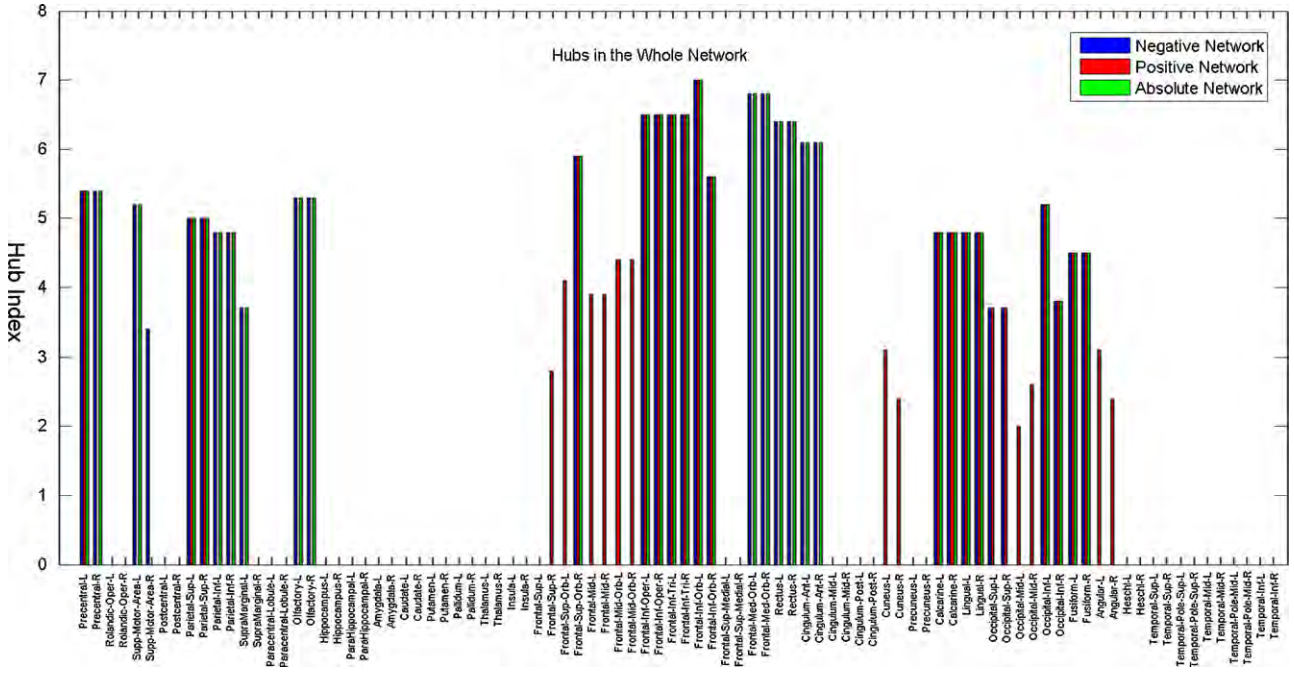

Fig. 6. Hub regions. Hub regions were identified in three kinds of networks via hub index as defined in formula (6). A region is considered as a hub region if and only if it appears in justified pairs (with 10–90% overlap) among the clustering results of graphs from all thresholds under investigation.

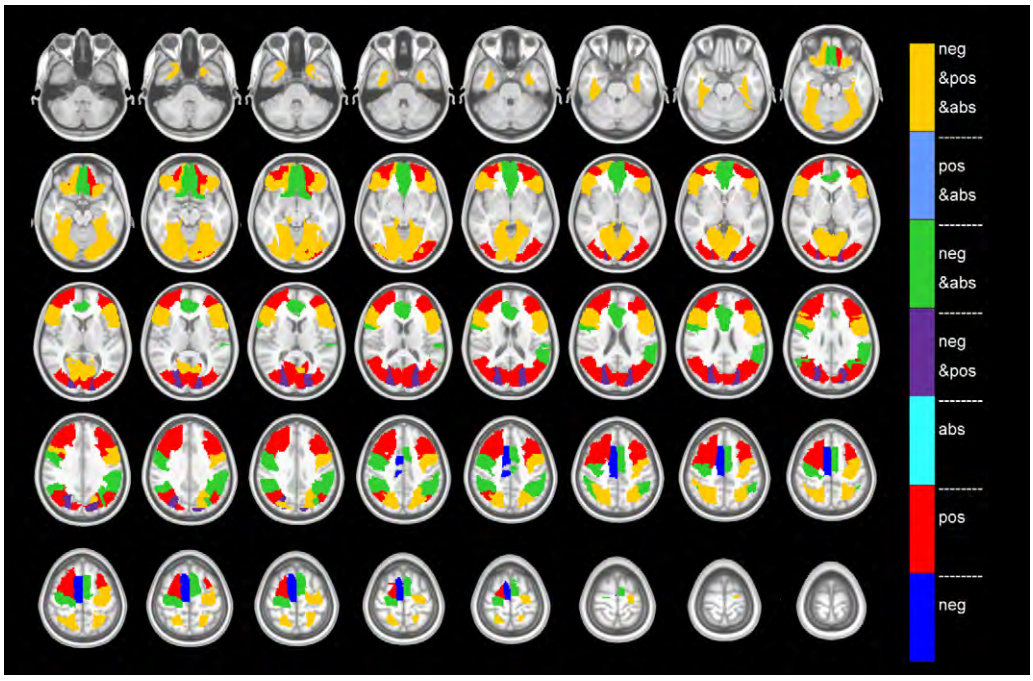

Fig. 7. Locations of the hub regions in the brain. Regions were labeled in different colors to indicate in which brain network they served as hubs. Abbreviations in the color bar follow that in Table 3. (For interpretation of the references to color in this figure legend, the reader is referred to the web version of the article.)

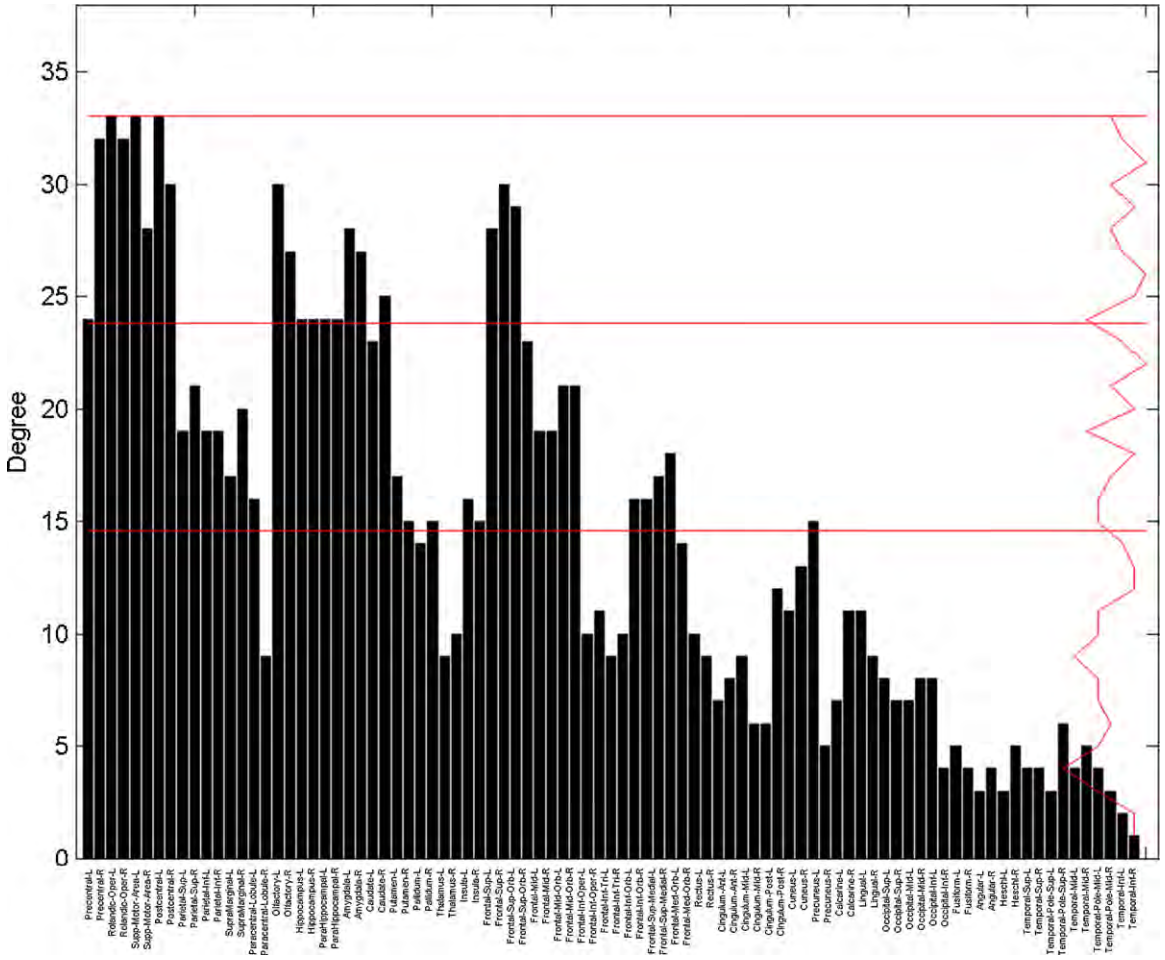

Fig. 8. The degree of each region in the whole brain network. The red horizontal lines are the algorithmic mean, one and two standard deviation above the algorithmic mean subsequently. The red plot on the rightmost side of the figure is the frequency distribution of degrees in this graph. Since the degree does not follow normal distribution, the use of algorithmic mean and standard deviation is putative rather than strict. (For interpretation of the references to color in this figure legend, the reader is referred to the web version of the article.)

Table 2
The clustering results and ROI membership in dataset 2. $K = 6$: in the K-means clustering method, the number of clusters was set to 6. CIS: the Connected Iterative Scan method.

ROI	Ref	$K = 6$	CIS
Precentral	Motor-Somatosensory	C1	C3,C6
Rolandic	Motor-Somatosensory	C2	C3,C6
SuppMotor	Motor-Somatosensory	C3	C3,C5
PostCentral	Motor-Somatosensory	C1	C3,C6
ParietalSup	Motor-Somatosensory	C1	C2,C3,C6
ParietalInf	Motor-Somatosensory	C1	C3,C6
SupraMarginal	Motor-Somatosensory	C1	C3,C6
Paracentral	Motor-Somatosensory	C1	C3
Olfactory		C1	C5,C6
Hippocampus	Emotion-memory	C1	C1,C6
ParaHipp	Emotion-memory	C2	C1,C6
Amygdala	Emotion-memory	C2	C1,C6
Caudate		C2	C1
Putamen		C2	C1
Pallidum		C2	C1
Thalamus		C2	C1
Insula		C4	C3,C6
Frontal-Sup	Frontal	C3	C4,C5
Frontal-Sup-Orb	Frontal	C2	C4,C5
Frontal-Mid	Frontal	C3	C4,C5,C6
Frontal-Mid-Orb	Frontal	C5	C4,C5
Frontal-Inf-Oper	Frontal	C4	C4,C5,C6
Frontal-Inf-Tri	Frontal	C1	C5,C6
Frontal-Inf-Orb	Frontal	C1	C5,C6
Frontal-Sup-Med	Frontal	C1	C4,C5
Frontal-Med-Orb	Frontal	C1	C4,C5
Rectus	Frontal	C1	C4,C5
Cingulum-Ant	Cingulate	C3	C4,C5
Cingulum-Mid	Cingulate	C3	C3
Cingulum-Post	Cingulate	C3	C4,C5
Cuneus	Cingulate	C4	C2,C4
Precuneus	Cingulate	C5	C2,C4
Calcarine	Visual	C3	C2
Lingual	Visual	C3	C2
Occipital-Sup	Visual	C6	C2
Occipital-Mid	Visual	C6	C2
Occipital-Inf	Visual	C4	C2
Fusiform	Visual	C4	C1,C2,C6
Angular	Visual	C4	C5,C6
Heschl	Visual	C4	
Temporal-Sup	Attention	C4	C6
Temporal-Pole-Sup	Attention	C3	C6
Temporal-Mid	Attention	C6	C6
Temporal-Pole-Mid	Attention	C5	C6
Temporal-Inf	Attention	C5	C6

Hub regions were also identified based on the overlap between clusters.

CIS replicated the known separation between the two anti-correlated networks in Set 1, while also casting light on the possible overlap between them. It has been reported that the brain contains two anti-correlation networks: one *task-positive network* which is activated during attention demanding goal-directed tasks (Toro et al., 2008), and one task-negative network which is deactivated during these tasks but active during resting state, also called the *default mode network* (Gusnard and Raichle, 2001; Raichle et al., 2001). The anti-correlation has been confirmed across different kinds of resting states (eyes closed, eyes open, with visual fixation) (Fox et al., 2005; Fransson, 2005), in meta-analysis (Toro et al., 2008), as well as in a large resting state dataset consisting 1414 subjects (Biswal et al., 2010). Results from the current study imply that there does not seem to be clear boundary between the two networks. Clustering via K-means ($K = 2$) grouped the posterior cingulate cortex into the *task-positive* network (red color in Fig. 4B) rather than the *default mode network* (yellow color in Fig. 4B), while the ventral frontal eye fields, the right dorsolateral prefrontal cortex, the left thalamus, the left ventral occipital cortex, and the right cerebellum were grouped into the *default mode network* rather than the task-positive network. Similar cross-grouping were also found in the clustering results of CIS, and CIS further revealed that the posterior cingulate cortex and the lateral parietal cortex were overlapping elements between the *task-positive* network (cluster 3) and the *default mode network* (cluster 1 and cluster 2). The lateral parietal cortex is reported to contain neurons for mediating eye movements driven by memory-guided attention (Kusunoki and Goldberg, 2003; Goldberg et al., 2006). The posterior cingulate cortex has been reported to serve important evaluative functions such as monitoring sensory events and the organism's own behavior (Vogt et al., 1992), and it was found to be a key region in the default mode network of resting state brain (Greicius et al., 2003), and also play an important role in allocation of attentional resources (Davis et al., 1997; Small et al., 2003). Consistent with their known function, our study shows that they are overlapped regions between the anti-correlated default mode network and the task positive network, promoting our understanding to their status in the architecture of brain neural network.

There have been found to be several functional clusters and functional sub-networks in the whole brain RSN, such as the motor network (Xiong et al., 1999), the sensorimotor, visual, language, and auditory clusters (Cordes et al., 2000b), the task-positive and default mode network (Raichle et al., 2001; Fox et al., 2005), which has been confirmed to correspond to the activated clusters involved in specific cognitive tasks (Smith et al., 2009). Similar functional clusters were also identified in the current study, including the visual cluster (cluster 2), the sensorimotor cluster (cluster 3), the frontal–cingulate cluster (cluster 4), and the hippocampus–amygdala cluster (cluster 1). Successful detection of these clusters further confirms the effectiveness of CIS. Additionally, overlapping was revealed. For instance, the fusiform cortex, a typical region for the visual cognition (cluster 2) (Kanwisher et al., 1997; Simons et al., 2003), appeared in the amygdala–hippocampus cluster (cluster 1). This is consistent with a previous report showing that the fusiform cortex plays an important role in the formation (Morris et al., 1999) and recapitulation (Fenker et al., 2005) of emotional memory. Two large clusters were detected. One includes the frontal, parietal, angular, olfactory and insular cortex and the hippocampus, amygdala (cluster 5), and the other includes the frontal, the temporal and the cingulate regions (cluster 6). Cluster 6 might reflect the hierarchy of these three overlapping functional systems. Cluster 5 may indicate the existence of a network for emotional memory. It has been known that emotion plays an important role in the formation and consolidation of memory, with the amygdala and the hippocampus playing a key role in this process (LeDoux, 1993; Hamann, 2001). The frontal and parietal regions, as well as the insula, have also been found to be critical for spatial and verbal working memory in a number of studies (D'Esposito et al., 1995, 1998; Smith et al., 1996; Hampson et al., 2006). The olfactory cortex, the angular cortex, and the postcentral cortex serve as the neural center for olfaction (Zatorre et al., 1992), language (Horwitz et al., 1998) and somatosensory (Drevets et al., 1995), respectively, in the human brain. They may serve as the sensory input to the emotional memory system in cluster 5, while the primary motor cortex (the precentral cortex) serves as the output of this system. Further investigation is required to test this hypothesis. In contrary, the clusters from K-means are rather small and fractional, unable to reflect the functional relationships among the brain regions. For instance, the frontal regions were separated into different clusters and the middle temporal pole was grouped into a visual cluster. In summary, CIS successfully detected the intrinsic functional clusters and sub-networks in RSN, while also revealing meaningful overlap between them.

Some regions play critical roles in the brain network by maintaining connections with many brain regions, thus have been called hub regions (Achard et al., 2006). Previous studies have identified

Table 3
Hub regions shown in Figs. 6 and 7.

Regions	$Index_{Hub}$		Networks	functional systems	Previous report
	L	R			
Cingulum_Ant	6.1	6.1	Neg&Abs	C	1,3,4
Cuneus	3.1	2.4	Pos	C	1,3
Frontal_Inf_Oper	6.5	6.5	Pos&Neg&Abs	F	
Frontal_Inf_Orb	7	5.6	Pos&Neg&Abs	F	1,4
Frontal_Inf_Tri	6.5	6.5	Pos&Neg&Abs	F	
Frontal_Med_Orb	6.8	6.8	Neg&Abs	F	4
Frontal_Mid	3.9	3.9	Pos	F	1,2,3,4
Frontal_Mid_Orb	4.4	4.4	Pos	F	1,2,4
Frontal_Sup_Orb_L	4.1	–	Pos	F	1,2,4
Frontal_Sup_Orb_R	–	5.9	Pos&Neg&Abs	F	1,2,4
Frontal_Sup_R	–	2.8	Pos	F	1,4
Olfactory	5.3	5.3	Neg&Abs	F	
Rectus	6.4	6.4	Neg&Abs	F	
Precentral_L	5.4	–	Pos&Neg&Abs	M	1,2
Precentral_R	–	5.4	Neg&Abs	M	1
Supp_Motor_Area	5.2	3.4	Neg&Abs	M	1
Parietal_Inf	4.8	4.8	Neg&Abs	P	1,3,4
Parietal_Sup	5	5	Pos&Neg&Abs	P	1,3,4
SupraMarginal	3.7	–	Neg&Abs	P	2,3,4
Angular	3.1	2.4	Pos	V	2
Calcarine	4.8	4.8	Pos&Neg&Abs	V	1,3
Fusiform	4.5	4.5	Pos&Neg&Abs	V	1
Lingual	4.8	4.8	Pos&Neg&Abs	V	1,2
Occipital_Inf	5.2	3.8	Pos&Neg&Abs	V	
Occipital_Mid	2	2.6	Pos	V	1
Occipital_Supp	3.7	3.7	Pos&Neg	V	1

Abbreviations: Pos: positive network, Neg: negative network, Abs: absolute network, C: cingulum, F: frontal, M: motor, P: parietal, and V: visual; 1: Achard et al. (2006), 2: He et al. (2008), 3: Hagmann et al. (2008), and 4: Buckner et al. (2009).

hub regions in the RSN (Achard et al., 2006) and the structural brain network (Hagmann et al., 2008) as well as the neural networks of cats and macaques (Sporns et al., 2007). Abnormality of hubs was also found in patients with Alzheimer's disease (He et al., 2008; Buckner et al., 2009). Many of the hub regions identified in this study were also reported in previous studies, as summarized in the last column of Table 3. Whereas previous hub index mainly reflected how much a region formed connections across the cortex, the hub index used in the current study reflected how actively a region participated in functional clusters, enabling us to capture the delicate architecture of the RSN. For instance, a region might have weak correlations with many brain regions and, as such, not have strong enough connections to form a cohesive cluster despite a large number of connections. Such a region will not be included as a hub because our $Index_{Hub}$ set threshold on correlation coefficients to as high as $r = 0.5$. Current knowledge in the field does not allow us to make comparison on the effect of different indexes to define the hub regions. Application of the above mentioned hub indexes in clinical studies will be able to show the advantage and disadvantage of each.

Currently, existing methods for partitioning fMRI data all emphasize the orthogonality, independence or disjointness among components, which is an assumption that is not strictly justified considering the nature of the neural network of the human brain. In the current study, CIS has been shown to be able to reveal the possible overlap between functional clusters in the brain and to identify hub regions in the neural network of human brain. Such capability is potentially useful in revealing the interleaving connectivity among the delicate architecture of the human brain neural network. Future studies will explore the performance of CIS in task activated brain networks and in clinical application.

Contributions

Study design: X.Y., M.G; data analysis: X.Y., S.K; manuscript writing: X.Y., S.K., B.B.

Acknowledgements

This study is based upon work partially supported by the U.S. National Science Foundation (NSF) under Grant Nos. IIS-0324947 and by the U.S. Department of Homeland Security (DHS) through the Center for Dynamic Data Analysis for Homeland Security administered through ONR grant number N00014-07-1-0150 to Rutgers University. The content of this paper does not necessarily reflect the position or policy of the U.S. government, no official endorsement should be inferred or implied. We thank Institute of Psychology of the Chinese Academy of Sciences for providing the fMRI dataset. We also thank Dr. John Rinzel at the Center for Neural Science, New York University for his encouragement and valuable comments on this study.

References

Achard S, Bullmore E. Efficiency and cost of economical brain functional networks. PLoS Comput Biol 2007;3:e17.
Achard S, Salvador R, Whitcher B, Suckling J, Bullmore E. A resilient, low-frequency, small-world human brain functional network with highly connected association cortical hubs. J Neurosci 2006;26:63–72.
Baumes J, Goldberg M, Magdon-Ismail M, Wallace W. Security informatics and terrorism: patrolling the web. In: Cecilia S. Gal PBK, Bracha Shapira, editors. NATO science for peace and security series, sub-series D: information and communication security; 2008.
Biswal B, Yetkin FZ, Haughton VM, Hyde JS. Functional connectivity in the motor cortex of resting human brain using echo-planar MRI. MRM 1995;34:537–41.
Biswal BB, Kylen JV, Hyde JS. Simultaneous assessment of flow and BOLD signals in resting-state functional connectivity maps. NMR Biomed 1997;10:165–70.
Biswal BB, Mennes M, Zuo X-N, Gohel S, Kelly C, Smith SM, et al. Toward discovery science of human brain function. PNAS 2010;107:4734–9.
Biswal BB, Pathak AP, Ulmer JL, Hudetz AG. Decoupling of the hemodynamic and activation-induced delays in functional magnetic resonance imaging. J Comput Assist Tomogr 2003;27:219.
Buckner RL, Sepulcre J, Talukdar T, Krienen FM, Liu H, Hedden T, et al. Cortical hubs revealed by intrinsic functional connectivity: mapping, assessment of stability, and relation to Alzheimer's disease. J Neurosci 2009;29:1860–73.
Calhoun VD, Adali T, Hansen LK, Larsen J, Pekar JJ. ICA of functional MRI data: an overview. Paper presented at the Proceedings of the International Workshop on Independent component Analysis and Blind Signal Separation Japan; 2003.

Cole DM, Smith SM, Beckmann CF. Advances and pitfalls in the analysis and interpretation of resting-state FMRI data. Front Syst Neurosci 2010;4:8.
Cordes D, Haughton V, Carew JD, Arfanakis K, Maravilla K. Hierarchical clustering to measure connectivity in fMRI resting-state data. Magn Reson Imaging 2002;20:305–17.
Cordes D, Haughton VM, Arfanakis K, Wendt GJ, Turski PA, Moritz CH, et al. Mapping functionally related regions of brain with functional connectivity MR imaging. Am J Neuroradiol 2000a;21:1636–44.
Cordes D, Haughton VM, Arfanakis K, Wendt GJ, Turski PA, Moritz CH, et al. Mapping functionally related regions of brain with functional connectivity MR imaging. AJNR Am J Neuroradiol 2000b;21:1636–44.
D'Esposito M, Aguirre GK, Zarahn E, Ballard D, Shin RK, Lease J. Functional MRI studies of spatial and nonspatial working memory. Cogn Brain Res 1998;7:1–13.
D'Esposito M, Detre JA, Alsop DC, Shin RK, Atlas S, Grossman M. The neural basis of the central executive system of working memory. Nature 1995;378:279–81.
Davis KD, Taylor SJ, Crawley AP, Wood ML, Mikulis DJ. Functional MRI of pain- and attention-related activations in the human cingulate cortex. J Neurophysiol 1997;77:3370–80.
Drevets WC, Burton H, Videen TO, Snyder AZ, Simpson JR, Raichle ME. Blood flow changes in human somatosensory cortex during anticipated stimulation. Nature 1995;373:249–52.
Fenker DB, Schott BH, Richardson-Klavehn A, Heinze HJ, Duzel E. Recapitulating emotional context: activity of amygdala, hippocampus and fusiform cortex during recollection and familiarity. Eur J Neurosci 2005;21:1993–9.
Fisher RA. Frequency distribution of the values of the correlation coefficient in samples of an indefinitely large population. Biometrika 1915;10:507–21.
Fortunato S. Community detection in graphs. Phys Rep 2009;486:75–174.
Fox MD, Snyder AZ, Vincent JL, Corbetta M, Van Essen DC, Raichle ME. The human brain is intrinsically organized into dynamic, anticorrelated functional networks. PNAS 2005;102:9673–8.
Fransson P. Spontaneous low-frequency BOLD signal fluctuations: an fMRI investigation of the resting-state default mode of brain function hypothesis. Hum Brain Mapp 2005;26:15–29.
Friston KJ. Functional and effective connectivity in neuroimaging: a synthesis. Hum Brain Mapp 1994;2:56–78.
Friston KJ, Rotshtein P, Geng JJ, Sterzer P, Henson RN. A critique of functional localisers. Neuroimage 2006;30:1077–87.
Goldberg M, Hayvanovych M, Hoonlor A, Kelley S, Magdon-Ismail M, Mertsalov K, et al. Discovery, analysis and monitoring of hidden social networks and their evolution. Paper presented at the IEEE Conference on Technologies for Homeland Security, 12–13 May 2008; 2008.
Goldberg M, Kelley S, Magdon-Ismail M, Mertsalov K, Wallace W. Finding Overlapping Communities in Social Networks. Paper presented at the 2010 IEEE International Conference on Social Computing, Minneapolis, MN, USA, August, 2010; 2010.
Goldberg ME, Bisley JW, Powell KD, Gottlieb J. Saccades, salience and attention: the role of the lateral intraparietal area in visual behavior. Prog Brain Res 2006;155:157–75.
Golland Y, Golland P, Bentin S, Malach R. Data-driven clustering reveals a fundamental subdivision of the human cortex into two global systems. Neuropsychologia 2008;46:540–53.
Gong G, He Y, Concha L, Lebel C, Gross DW, Evans AC, et al. Mapping anatomical connectivity patterns of human cerebral cortex using in vivo diffusion tensor imaging tractography. Cereb Cortex 2009;19:524–36.
Goutte C, Toft P, Rostrup E, Nielsen FA, Hansen LK. On clustering fMRI time series. Neuroimage 1999;9:298–310.
Greicius MD, Krasnow B, Reiss AL, Menon V. Functional connectivity in the resting brain: a network analysis of the default mode hypothesis. PNAS 2003;100:253–8.
Gusnard DA, Raichle ME. Searching for a baseline: functional imaging and the resting human brain. Nat Rev Neurosci 2001;2:685–94.
Hagmann P, Cammoun L, Gigandet X, Meuli R, Honey CJ, Wedeen VJ, et al. Mapping the structural core of human cerebral cortex. PLoS Biol 2008;6:e159.
Hamann S. Cognitive and neural mechanisms of emotional memory. Trends Cogn Sci 2001;5:394–400.
Hampson M, Driesen NR, Skudlarski P, Gore JC, Constable RT. Brain Connectivity Related to Working Memory Performance. J Neurosci 2006;26:13338–43.
He Y, Chen Z, Evans A. Structural insights into aberrant topological patterns of large-scale cortical networks in Alzheimer's disease. J Neurosci 2008;28:4756–66.
Horwitz B, Rumsey JM, Donohue BC. Functional connectivity of the angular gyrus in normal reading and dyslexia. PNAS 1998;95:8939.
Kanwisher N, McDermott J, Chun MM. The fusiform face area: a module in human extrastriate cortex specialized for face perception. J Neurosci 1997;17:4302.
Kusunoki M, Goldberg ME. The time course of perisaccadic receptive field shifts in the lateral intraparietal area of the monkey. J Neurophysiol 2003;89:1519–27.
Lancichinetti A, Fortunato S. Community detection algorithms: a comparative analysis. Phys Rev E 2009;80:056117.
Lancichinetti A, Kivelä M, Saramäki J, Fortunato S. Characterizing the community structure of complex networks. PLoS ONE 2010;5:e11976.
LeDoux JE. Emotional memory systems in the brain. Behav Brain Res 1993;58:69–79.
Li SJ, Biswal B, Li Z, Risinger R, Rainey C, Cho JK, et al. Cocaine administration decreases functional connectivity in human primary visual and motor cortex as detected by functional MRI. Magn Reson Med 2000;43:45–51.
Margulies DS, Kelly AMC, Uddin LQ, Biswal BB, Castellanos FX, Milham MP. Mapping the functional connectivity of anterior cingulate cortex. Neuroimage 2007;37:579–88.
McKeown MJ, Makeig S, Brown GG, Jung TP, Kindermann SS, Bell AJ, et al. Analysis of fMRI data by blind separation into independent spatial components. Hum Brain Mapp 1998;6:160–88.
Morgan VL, Gore JC, Szaflarski JP. Temporal clustering analysis: what does it tell us about the resting state of the brain? Med Sci Monit 2008;14:CR345–52.
Morris JS, Ohman A, Dolan RJ. A subcortical pathway to the right amygdala mediating unseen fear. PNAS 1999;96:1680.
Oja E, Hyvarinen A. Independent component analysis: algorithms and applications. Neural Netw 2000;13:411–30.
Raichle ME, MacLeod AM, Snyder AZ, Powers WJ, Gusnard DA, Shulman GL. A default mode of brain function. PNAS 2001;98:676–82.
Saad ZS, Ropella KM, Cox RW, DeYoe EA. Analysis and use of fMRI response delays. Hum Brain Mapp 2001;13:74–93.
Simons JS, Koutstaal W, Prince S, Wagner AD, Schacter DL. Neural mechanisms of visual object priming: evidence for perceptual and semantic distinctions in fusiform cortex. Neuroimage 2003;19:613–26.
Small DM, Gitelman DR, Gregory MD, Nobre AC, Parrish TB, Mesulam MM. The posterior cingulate and medial prefrontal cortex mediate the anticipatory allocation of spatial attention. Neuroimage 2003;18:633–41.
Smith EE, Jonides J, Koeppe RA, Dissociating Verbal. Spatial working memory using PET. Cereb Cortex 1996;6:11–20.
Smith SM, Fox PT, Miller KL, Glahn DC, Fox PM, Mackay CE, et al. Correspondence of the brain's functional architecture during activation and rest. PNAS 2009;106:13040–5.
Spath H. Cluster dissection and analysis: theory, FORTRAN programs examples. New York: Halsted Press; 1985.
Sporns O, Honey CJ, Koter R. Identification and classification of hubs in brain networks. PLoS One 2007;2.
Stanberry L, Nandy R, Cordes D. Cluster analysis of fMRI data using dendrogram sharpening. Hum Brain Mapp 2003;20:201–19.
Stein T, Moritz C, Quigley M, Cordes D, Haughton V, Meyerand E. Functional connectivity in the thalamus and hippocampus studied with functional MR imaging. AJNR Am J Neuroradiol 2000;21:1397–401.
Supekar K, Menon V, Rubin D, Musen M, Greicius MD. Network analysis of intrinsic functional brain connectivity in Alzheimer's disease. PLoS Comput Biol 2008;4:e1000100.
Supekar K, Musen M, Menon V. Development of large-scale functional brain networks in children. PLoS Biol 2009;7:e1000157.
Talairach J, Tournoux P. Co-planar stereotaxic atlas of the human brain: 3-dimensional proportional system: an approach to cerebral imaging. New York, USA: Thieme; 1988.
Toro R, Fox PT, Paus T. Functional coactivation map of the human brain. Cereb Cortex 2008;18:2553–9.
Tzourio-Mazoyer N, Landeau B, Papathanassiou D, Crivello F, Etard O, Delcroix N, et al. Automated anatomical labeling of activations in SPM using a macroscopic anatomical parcellation of the MNI MRI single-subject brain. Neuroimage 2002;15:273–89.
Vogt BA, Finch DM, Olson CR. Functional heterogeneity in cingulate cortex: the anterior executive and posterior evaluative regions. Cereb Cortex 1992;2:435.
Wang L, Zhu C, He Y, Zang Y, Cao Q, Zhang H, et al. Altered small-world brain functional networks in children with attention-deficit/hyperactivity disorder. Hum Brain Mapp 2009;30:638–49.
Xiong J, Parsons LM, Gao JH, Fox PT. Interregional connectivity to primary motor cortex revealed using MRI resting state images. Hum Brain Mapp 1999;8:151–6.
Zatorre RJ, Jones-Gotman M, Evans AC, Meyer E. Functional localization and lateralization of human olfactory cortex. Nature 1992.